Ultrafiltration conducting membranes and coatings from redispersable, nanoscaled, crystalline SnO_2:Sb particles†

Christian Goebbert,[a] Michel A. Aegerter,*[a] Detlef Burgard,[b] Ruediger Nass[b] and Helmut Schmidt[b]

Institut für Neue Materialien-INM, [a]Department of Coating Technology, [b]Department of Chemistry and Technology of Nonmetallic–Inorganic Materials, D-66123 Saarbruecken, Germany. E-mail: aegerter@inm-gmbh.de

Inorganic membranes prepared by the sol–gel method are promising candidates for use as filters in separation processes. Conducting supported membranes and coatings have been produced from redispersable nanoscaled crystalline Sb-doped SnO_2 powders with Sb contents up to 10 mol%. The crystalline particles (*ca.* 4 nm) are fully redispersable in aqueous solution at pH $\geqslant$ 8 with a solid content up to 37 vol.% and are monosized. After thermal treatment at different temperatures and times, the pore size diameter of such a powder can be adjusted from 4–20 nm with a very narrow pore size distribution (*ca.* ± 1 nm) and a total porosity of 63%, practically independent of the sintering parameters. Uniaxial compacted substrates (unsupported membranes) present similar characteristics but with a larger pore size distribution (± 5 nm) and 80% total porosity. Their electrical resistance decreases with sintering temperature and time to 4 Ω (800 °C, 8 h). Crack free transparent conducting coatings on glasses and ceramics have been obtained by spin-coating using fully dispersed aqueous solutions of the powder with volume content up to 7.8%. After thermal treatment (1 h at 550 °C) single layers 200 nm thick are still porous and exhibit specific electrical resistivity as low as $\rho = 2.5 \times 10^{-2}$ Ω cm with 90% transmission in the visible range.

Introduction

There is growing interest in microbiological resistant and chemically stable materials in the development of membranes for separation processes. Polymeric materials deteriorate above 200 °C or in the presence of organic solvents and do not always have the desired porous texture. Ceramic materials (such as alumina, silica, titania, zirconia, *etc.*) fulfil these requirements and are presently used in the preparation of membranes for microfiltration, ultrafiltration and hyperfiltration with pore sizes ranging between 100 and 1000 nm, 2 and 100 nm and <2 nm respectively.[1]

The sol–gel process is a versatile technique for the preparation of ceramic membranes as it allows the control of the pore size and pore distribution.[2] The major problem lies in the obtention of thick coatings (>1 μm) which may crack during the postsynthesis drying and sintering stages.

Sol–gel research in the field of micro and ultrafiltration membranes has principally involved alumina (Al_2O_3) and silica (SiO_2) materials[3–7] and transition metal oxides such as TiO_2 and ZrO_2.[7–9] However, it has been recently shown that SnO_2 also has appropriate microstructural characteristics for such applications.[10–12] The sols used for membrane preparation were aqueous colloidal suspensions (alkaline solution) containing spheroidal primary particles of 2 nm average size obtained from an aqueous solution of tin chloride. Supported membranes have been realised using the sol-casting process on either micro or nanoporous α-Al_2O_3 with subsequent drying at 110 °C and firing at 400 °C for 2 h.[11,12] Crack-free membranes were only found within a narrow concentration range of SnO_2 and electrolyte in the sol.

A novel and promising process for the obtention of oxide membranes for ultrafiltration and optical coatings is presented in this paper. The fabrication of advanced nanostructured membranes and ceramics requires high quality powders and

their redispersability is a particularly important aspect. In a conventional synthesis, the intermediate particulate system minimizes its surface free energy by growing into larger particles which tend to agglomerate. These reactions can be avoided by adjusting the particles' surface free energy by *in-situ* surface modification during the precipitation and the controlled growth processes so that unagglomerated particles with a determined size can be prepared. The basic principle of the method is shown schematically in Fig. 1 and compared to the now classical sol–gel process which leads to irreversible formation of gels or agglomerated powders. This process is outlined for SnO_2 and electrically conducting SnO_2:Sb materials, both are wide band semiconductors and SnO_2:Sb is a good electronic conductor presenting a specific resistivity as low as 1×10^{-3} Ω cm.[13] The combination of conductivity and photocatalytic properties may be an asset for the development of membranes for hybrid processes. The paper describes the preparation and characterisation of redispersable, nanoscaled crystalline powders,[14] unsupported membranes, thin and thick coatings made by the spin coating process.

Experimental procedure

Powder preparation

SnO_2 (TO) and SnO_2:Sb (ATO) particles were prepared by a controlled growth technique.[15–17] A scheme of the process is shown in Fig. 2. A solution of tin(IV) chloride in ethanol containing up to 10 mol% $SbCl_3$ was added dropwise to an aqueous ammonia solution containing 10 wt.%, with respect to the oxide, of a surface modifying agent, β-alanine. The prepared suspensions were then treated in an autoclave at 150 °C and 10 bar for 3 h. The resulting powder, with its surface chemically modified in such a way that the particles do not agglomerate, was isolated by centrifugation, washed with water several times and then dried at 60 °C. Such a powder can be either fully redispersed in water at pH $\geqslant$ 8 under ultrasonic irradiation and the stable sol then deposited by spin coating on a glass substrate (transparent conducting
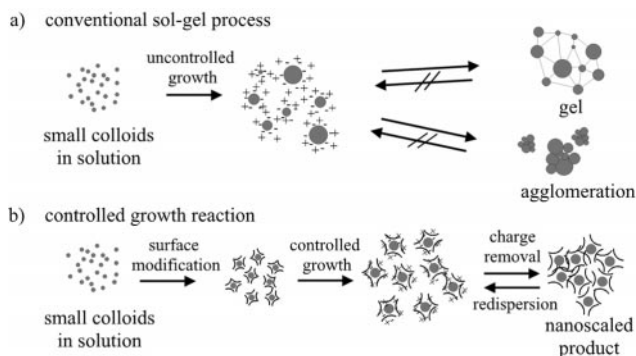
Fig. 1 Basic principle of powder preparation.
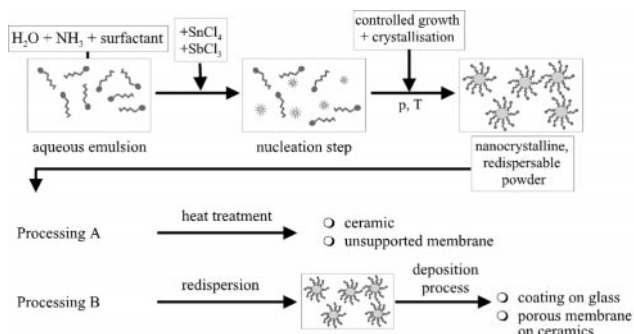

Fig. 2 SnO$_2$ and SnO$_2$:Sb processing.

coating) or on porous ceramics (supported conducting membrane), or used to prepare ceramics bodies such as unsupported membranes.

The size of the particles was measured by photon correlation spectroscopy (PCS) using an ALV-5000 instrument and high resolution transmission electron microscopy (HRTEM). The analysis of the pore characteristics of the loose powder thermally treated at different temperatures (400–800 °C) and times (10, 30, 90, 300 min) was performed by BET measurement (ASAP2400, Micromeritics). The powders were also characterised by X-ray diffraction (XRD) and density measurement with a pycnometer (AccuPyc1330, Micromeritics).

Unsupported membrane preparation

Pellets in the form of round discs, 38 mm in diameter and 1.8 mm thick, were uniaxially pressed under 100 kN pressure. They were then thermally heat treated in air at temperatures between 300 and 800 °C with sintering times of 0.5, 1, 4 and 8 h. The analysis of the pore characteristics was performed by BET measurement (ASAP2400, Micromeritics). The crystal structure of the pellets was determined by X-ray diffraction and their true density by pycnometer measurement (AccuPyc1330, Micromeritics). Their electrical resistance was measured by a two-point technique across their thickness.

Coating preparation

Colloidal suspensions were prepared by dispersing the non-thermally treated powder in water at pH $\geqslant$ 11 using 0.78 mol l^{-1} tetramethylammonium hydroxide (TMAH) as a base. After powder addition the resulting suspensions were submitted to ultrasonication for 2 min. After this treatment the suspensions were stirred for one day. The final dispersions were clear with a yellow–orange colour. Stable suspensions can be obtained up to a solid content of 37 vol.%.

Conducting coatings have been prepared on borofloat glass or alumina substrates using the spin coating process. At a final speed of 2500 rpm for 15 s crack-free spin coated coatings could be obtained with a solid content up to 7.7 vol.%. The

thermal densification of the film was carried out at temperatures from 400–600 °C for 0.25 to 8 h. The film thickness was measured with a Tencor P10 surface profiler. The characterisation of the electrical properties was carried out by the four-point and van der Pauw/Hall techniques (MMR Technologies) and the coating texture was analyzed by HRTEM and atomic force microscopy (AFM).

Results and discussion

Powder characterisation

X-Ray diffraction patterns of the dried SnO$_2$ and SnO$_2$:Sb powders are shown in Fig. 3. The particles are already crystalline and have a cassiterite structure. The vertical lines correspond to the data taken from the JCPDS files for this structure. They are not orientated and have a crystallite size, calculated with Siemens software for the (110) peak, of 7 nm for SnO$_2$ and 3 nm for Sb doped SnO$_2$. A systematic decrease in crystallite size was observed with increasing antimony content.

The hydrodynamic size distribution of the particles measured by PCS is narrow with a maximum at 4 nm. The size of the particles was confirmed by HRTEM (Fig. 4) which shows crystalline particles with an average size of 3 to 5 nm with no evidence of aggregation. Each particle seems to be formed by a single crystallite.

The evolution of the powder porosity after different heat treatment is shown in Fig. 5 where the N$_2$ adsorption and
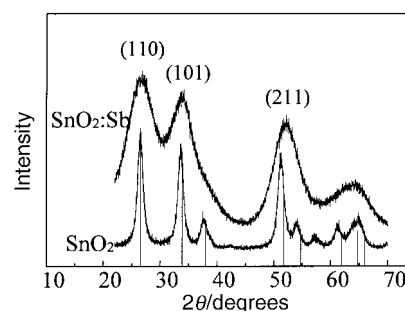

Fig. 3 X-Ray diffraction patterns of dried SnO$_2$ and SnO$_2$:Sb (5 mol %) nanoscaled, crystalline powder prepared by a controlled growth reaction at 150 °C and 10 bar for 3 h.
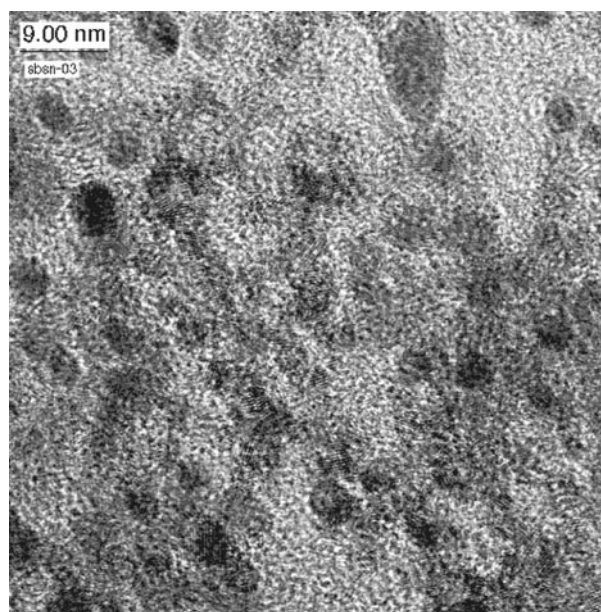

Fig. 4 HRTEM picture of nanocrystalline SnO$_2$:Sb powder obtained by a controlled growth reaction and hydrothermal crystallisation at 150 °C and 10 bar for 3 h, redispersed in water and TMAH.
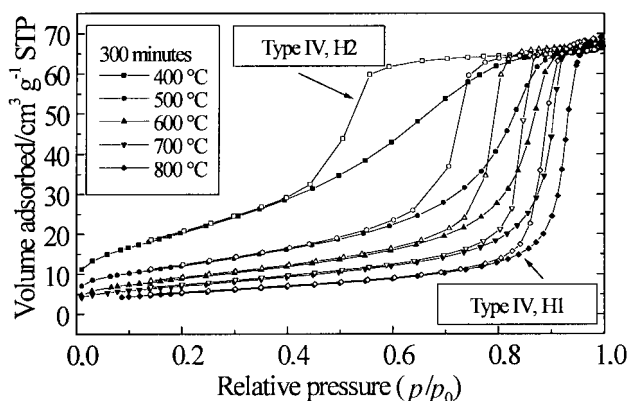
Fig. 5 N₂ adsorption and desorption isotherms of $SnO_2:Sb$ powder heat treated at different temperatures during 5 h (solid symbols = adsorption; open symbols = desorption).

Fig. 7 Influence of temperature and sintering time on the BET surface area and the true density of $SnO_2:Sb$ powder ($\bullet/\circ$ 400 °C, $\blacksquare/\square$ 500 °C, $\blacktriangle/\triangle$ 600 °C, $\blacktriangledown/\triangledown$ 700 °C, $\blacklozenge/\lozenge$ 800 °C; solid symbols = BET surface; open symbols = density).

desorption isotherms are compared. According to the IUPAC classification,[18] the BET isotherms have a type IV shape at all temperatures. The hysteresis is of type H2 at low temperature and typical for capillary condensation inside ink-bottle shaped mesopores of porous systems. At high sintering temperatures the hysteresis tends towards a H1 type indicating a greater regularity of the cross section along the longitudinal direction of the pores (transformation of an ink-bottle shape towards a cylindrical shape[10]).

The pore size distribution curves were determined from the desorption branches. Fig. 6 indicates a strong increase of the pore size with the temperature of the heat treatment. For 400 °C, 10 min (or lower temperature) the pore size distribution is large showing the presence of micropores. Upon increasing the sintering temperature, the pore size distribution becomes narrower, about ±1 nm, and the average diameter shifts from 4 nm (400 °C) to 15–20 nm (800 °C) while the maximum pore volume remains constant with a value of about 0.75 cm³ g⁻¹. A longer sintering time gives a better defined pore size distribution with a slight shift of their size. This overall behaviour of the evolution of the pore size distribution has already been observed with undoped SnO_2 xerogel.[10] However, there are some interesting differences. For SnO_2:Sb prepared by a controlled growth reaction, the pore volume is always higher than that of SnO_2 xerogel, especially for the distribution at 400 °C and for those at $T \geqslant 700$ °C. At 700 °C the maximum pore volume of undoped SnO_2 xerogel is already strongly reduced to about 0.15 cm³ g⁻¹ and at 800 °C it is not measurable, while for SnO_2:Sb the volume is still high at 0.75 cm³ g⁻¹. It is not yet clear whether this behaviour is due to the antimony

doping or to the different methods of preparation of the materials. SnO_2:Sb is therefore more useful for the formation of membranes, where the pore diameter can be continuously adjusted with the sintering temperature and time with a narrow distribution in the range of 4 to 20 nm. The total porosity of the powder is 63%, and is practically independent of the sintering conditions.

Fig. 7 shows the influence of the sintering temperature and time on the BET surface area and true density of the SnO_2:Sb powder. The 60 °C dried powder, which was prepared in an autoclave at 150 °C, has a BET surface area of 220 m² g⁻¹ and a true density of 4 g cm⁻³. With the increase of the temperature and the sintering time the surface area decreases and reaches a minimum for each temperature for sintering times longer than about 300 min. The large decrease of the BET surface area at 400 °C is due partly to the gradual removal of the organic compound from the surface of the particles and partly to the removal of the microporosity (Fig. 6). At higher temperature the reduction of the BET surface area with the sintering time is smaller and in agreement with the change of the isotherm from type IV-H2 to type IV-H1 (better regularity). The true density increases in parallel with the sintering temperature and time and reaches at 700 °C (300 min) or 800 °C (100 min) values close to the theoretical density. The overal behaviour is in agreement with the results found by Santilli *et al.*[19] for SnO_2 xerogel, indicating that the sintering behaviour of SnO_2:Sb obeys a dynamic scaling model as for SnO_2 and that this material can be seen as a two-phase system composed a nearly homogeneous SnO_2:Sb matrix with high concentration of vacancies and empty microvoids. The total volume fraction of both phases (63% for the porous phase, 37% for the solid phase) remains constant at least up to 800 °C and the solid fraction reaches the theoretical value of the density at high temperatures (800 °C, 100 min). Under these conditions no significant bulk densification occurs in this temperature range, confirming the great interest of this material for the realisation of ultrafiltration membranes.

Without heat treatment the dried SnO_2:Sb powder is already crystalline with a crystallite size of *ca.* 4 nm as shown by X-ray diffraction, HRTEM and PCS measurements. After heating at 400 °C for 10 min, the crystallite size is smaller (*ca.* 2.5 nm; Fig. 8). It is thought that this reduction is due to the elimination of the microporosity (Fig. 7). Another proof of this is the increase of the density from 4–5.8 g/cm³ (Fig. 7). The size of the crystallites then increases with temperature and sintering time up to values of 20 nm (800 °C, 300 min). The particle size G can be evaluated using specific surface and density data [eqn. (1)] where S_{BET} is the surface area in m² g⁻¹, ρ the true density in g cm⁻³ (both taken from Fig. 7) and f is a coefficient
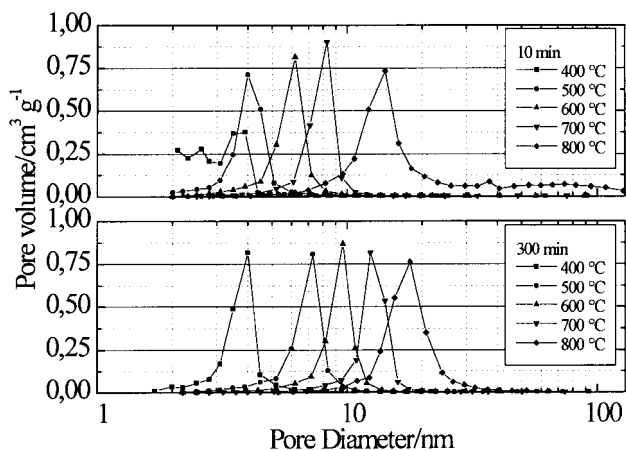

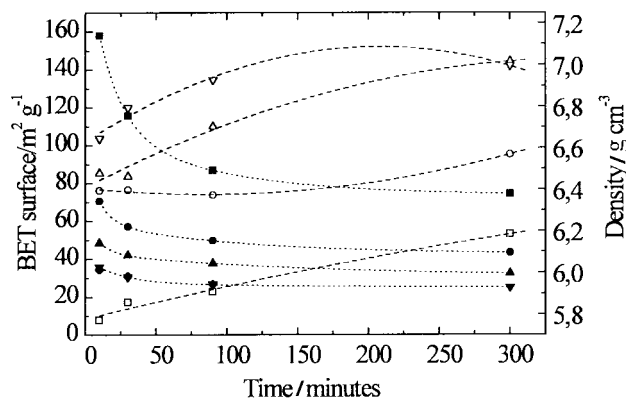**Fig. 6** Evolution of pore characteristics (volume, size) of loose powder with sintering temperature and time.
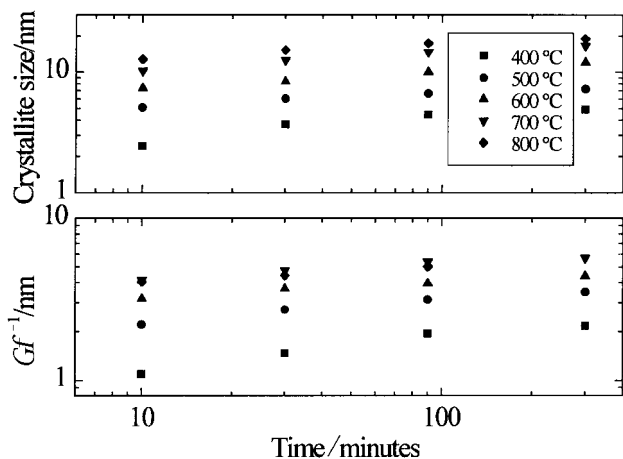
Fig. 8 Influence of temperature and sintering time on the crystallite size obtained from X-ray diffraction and plot of the G/f function (see text) calculated from specific surface area and true density measurement.

which depends on the shape and the distribution of the particles (up to 6 for cubes or spheres of identical distribution).

$$G \text{ (nm)} = f \times 10^{-3} [S_{\text{BET}}(T,t) \times \rho(T,t)]^{-1} \quad (1)$$

Fig. 8 shows also a plot of G/f vs. sintering time. The overall behaviour is identical to that of the crystallite size. Crystallites and particles appear therefore to grow following the same law. For sintering time $t \geqslant 30$ min the size grows as $D(t) = kt^n$ where n is smaller than 1, the value expected for the classical crystallite growth mechanism, confirming the special behaviour of tin oxide.

Unsupported membranes

The overall behaviour of the N_2 adsorption and desorption isotherms of uniaxial compacted substrates is similar to that presented for the loose powder shown in Fig. 5. The isotherms are of type IV with H2 hysteresis transforming into H1 type hysteresis at high temperatures (800 °C). The pore size also varied from 4 to 20 nm depending on the sintering time and temperature, but the distribution is larger (*ca.* ±5 nm) and the total porosity is higher (80%; Fig. 9). The true density increases and the BET surface area decreases in a similar way to loose powder (Fig. 10).

The electrical resistance of the pellets strongly decreases with increasing sintering temperature and time (Fig. 11). Dried pellets have a very high electrical resistance. With higher temperature and sintering time it decreases from 360 kΩ
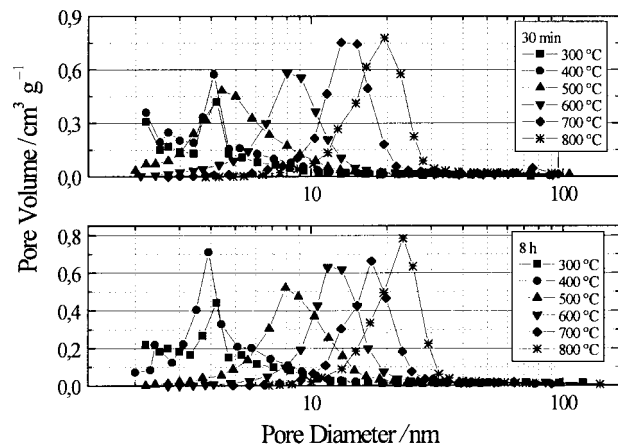

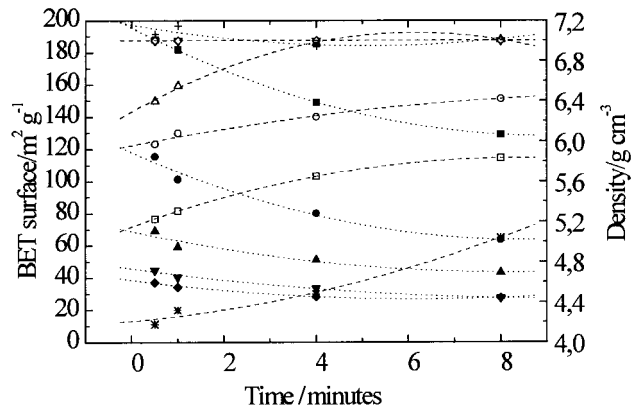Fig. 9 Evolution of pore characteristics (volume, size) of the pellets with sintering temperature and time.

Fig. 10 Influence of temperature and sintering time on the BET surface area and the true density of SnO_2:Sb pellets (●/○ 400 °C, ■/□ 500 °C, ▲/△ 600 °C, ▼/▽ 700 °C, ◆/◇ 800 °C; solid symbols = BET surface; open symbols = density).

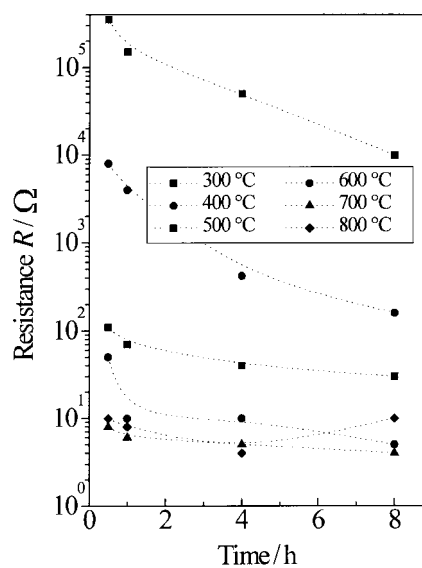Fig. 11 Change of the electrical resistance of pressed SnO_2:Sb substrates *versus* sintering time for different sintering temperatures.

(300 °C, 30 min) to 4 Ω (700 °C, 8 h). These values are higher than those obtained with coatings (see below).

Sol for coating

For the preparation of porous coatings using nanoscaled crystalline particles, the powder was redispersed in water. The stability of the dispersion was determined by measuring the ζ potential and is strongly dependent on the pH of the solvent. The isoelectrical point of the surface modified powder lies at a pH_{iep} of 3.7 and the potential values are negative and constant for pH > 5. No evidence for instability could be found with solid contents up to 14.3 vol.% for pH > 8.

With increasing particle concentration, the sol viscosity increases (Fig. 12) due to interactions between the particles but evidence for the formation of aggregates has not been found up to 14.3 vol.%.

Film characterisation

Films were prepared on glass and alumina substrates using the spin coating technique. Each film was densified in a furnace immediately after the spin coating process. The thickness of single layers increases with the particle concentration (Fig. 12) and this reflects the viscosity behaviour. Thicknesses as high
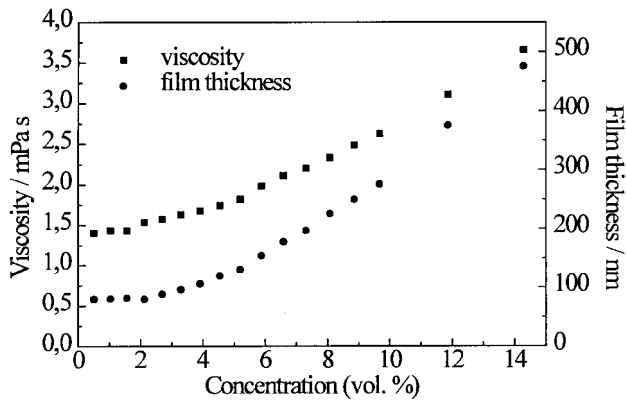
Fig. 12 Viscosity of the sol and thickness of spin coated single layers sintered at 550 °C during 15 min *vs.* SnO$_2$:Sb particle concentration of the sol.

Fig. 14 Optical transmission of a single layer sintered at 550 °C during 1 h, measured against air.

as 500 nm can be obtained for a single layer. Thicker coatings can be prepared by repeating the coating and sintering process.

The lowest resistivities were achieved with a 7.7 vol.% solid content of the powder in the sol. At higher concentrations the films start to crack and the resistivity increases. With this concentration single layers have a thickness of 200 nm after firing. As for the compacted substrate, the electrical resistance of the films depends on the temperature and time of the sintering process. Fig. 13 shows the resistivity of 200 nm thick single layers sintered at different temperatures and times. The lowest resistivity, 2.5×10^{-2} Ω cm, was obtained after sintering at 550 °C during 1 h. The coating has an electron mobility $\mu = 1$ cm^{-2} V s^{-1} and an electron density $n = 2.15 \times 10^{20}$ cm^{-3}. The coatings are highly transparent in the visible range with a transmission of 85–90% (Fig. 14). A HRTEM cross-section of a multi-layer coating is shown in Fig. 15. It is made of interconnected particles, assembled in a porous structure. A denser layer (*ca.* 20 nm thick) is observed on top of each layer. This layer has a higher conductivity than the bulk of the coating.[20] However, if each layer is dried at 150 °C between each deposition and the multilayer coating sintered as a whole at higher temperature, these denser layers do not occur and the coating is homogeneous. The resistivity of the coatings is much lower than those of the compacted substrates. Although their structure is still porous the coatings have probably a smaller total porosity. Such measurements are under way. AFM measurements show that the coating surface is smooth with a roughness typically less than 3 nm and no evidence of cracks or peel-off from the glass substrate on a 2 nm scale has been observed.
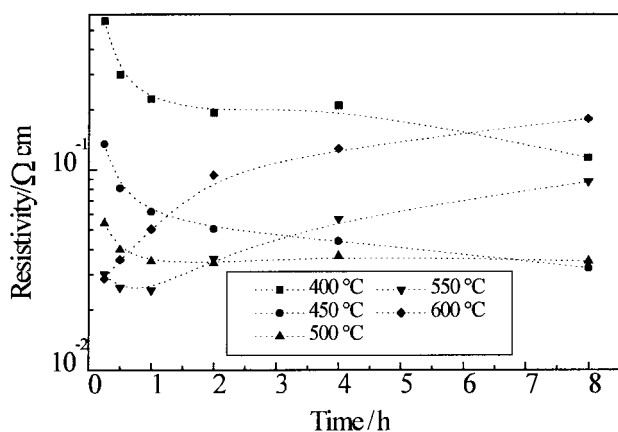

Fig. 13 Resistivity *vs.* sintering time for different sintering temperatures. Films were made with a 5.9 vol.% particle concentration in the sol.
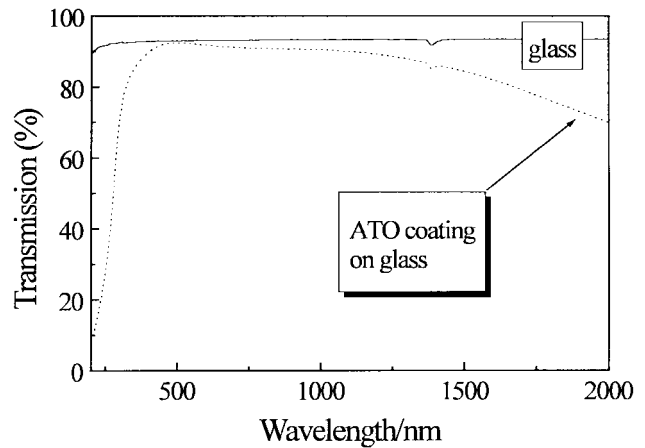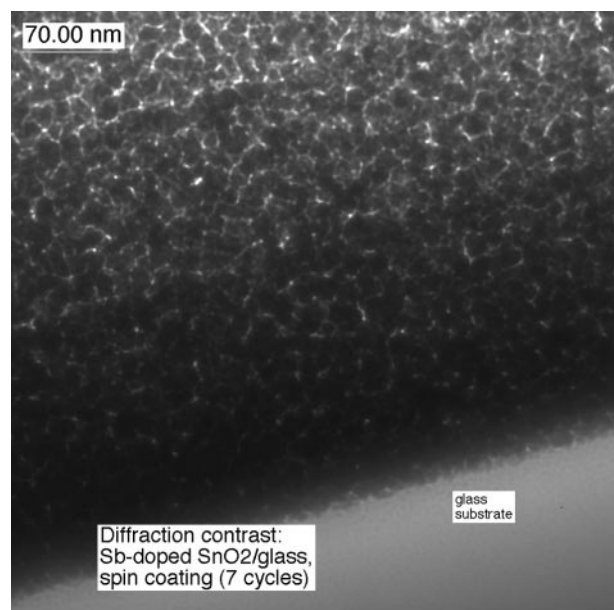

Fig. 15 Cross-section of a multi-layer SnO$_2$:Sb coating deposited by spin coating on a glass substrate with a particulate sol having a solid content of 7.7 vol.%. Each layer was sintered in air at 550 °C during 15 min.

Conclusion

Nanoscaled, crystalline SnO$_2$ and SnO$_2$:Sb particles which are fully redispersable in water have been prepared. The growth of the particles in solution was controlled by chemical modification of the particle surface using β-alanine. Dried powders can be fully redispersed in water at a nanoscale level. Suspension with solid contents up to 37 vol.% are stable for pH > 8. Thick coatings (up to 0.5 μm per layer) have been obtained by the spin coating process. The specific resistivity of SnO$_2$:Sb coatings depends on the thickness, the particle concentration, the temperature and time of the sintering process. Resistivity values as low as $\rho = 2.5 \times 10^{-2}$ Ω cm with a sheet resistance of $R_{\square} = 60$ Ω$_{\square}$ have been obtained for a 7 layer coating (thickness 1.4 μm). Loose powders heat treated in air exhibit microporosity with a narrow pore size distribution (± 1 nm). The pore size can be continuously varied in a controlled way between 4 nm (400 °C) and 20 nm (800 °C). Uniaxial pressed unsupported membranes show similar characteristics. The pore size distribution is however higher (± 5 nm) and the total porosity is 80%. The electrical resistance of these membranes typically varies from 360 kΩ (400 °C) to 4 Ω

(800 °C). These materials offer high chemical and thermal resistance and is therefore promising for industrial preparation of conducting membranes for ultrafiltration and transparent conducting layers for antistatic applications, or for systems which need sheet resistances larger than about 100 $\Omega_\square$, such as touch screen panels.

References

1   R. R. Bhave, *Inorganic Membranes: Synthesis, Characteristics and Application*, Van Nostrand Reinhold, New York, 1991.
2   C. J. Brinker and G. W. Scherer, *Sol–Gel Science: The physics and chemistry of sol-gel processing*, Academic Press Inc., San Diego, USA, 1990.
3   A. F. M. Leenaars, K. Keizer and A. J. Burggraaf, *J. Mater. Sci.*, 1984, **19**, 1077.
4   A. Larbot, S. Alami-Younssi, M. Persin, J. Sarrazin and L. Cot, *J. Membr. Sci.*, 1994, **97**, 167.
5   M. I. D. d. Albani and C. P. Arciprete, *J. Membr. Sci.*, 1992, **69**, 21.
6   C. J. Brinker, N. K. Raman, M. N. Logan, R. Sehgal, R. A. Assink, D. W. Hua and T. L. Ward, *J. Sol–Gel Sci. Technol.*, 1995, **4**, 117.
7   L. C. Klein, C. Yu, R. Woodman and R. Pavlik, *Catal. Today*, 1992, **14**, 165.
8   A. Larbot, J. P. Fabre and L. Cot, *J. Am. Ceram. Soc.*, 1989, **72**, 257.
9   C. Guizard, A. Julbe, A. Larbot and L. Cot, *J. Alloys Compd.*, 1992, **8**, 188.
10 G. E. S. Brito, S. H. Pulcinelli and C. V. Santilli, *J. Sol–Gel Sci. Technol.*, 1994, **2**, 575.
11 L. R. B. Santos, S. H. Pulcinelli and C. V. Santilli, *J. Sol–Gel Sci. Technol.*, 1997, **8**, 477.
12 L. R. B. Santos, S. H. Pulcinelli and C. V. Santilli, *J. Membr. Sci.*, 1997, **127**, 77.
13 G. Gasparro, J. Pütz, D. Ganz and M. A. Aegerter, *Proc. EuroSun'96 International Symposium on Optical Materials Technology for Energy Efficiency and Solar Energy Conversion*, Freiburg, 1996, in *Solar Energy Materials and Solar Cells*, 1998, **54**, 287.
14 D. Burgard, C. Goebbert and R. Nass, *J. Sol–Gel Sci. Technol.* in press.
15 D. Burgard, R. Nass and H. Schmidt, *MRS 432, Aqueous Chemistry and Geochemistry of Oxides, Oxyhydroxides and related Materials*, ed. J. A. Voigt, T. E. Wood, B. C. Bunker, W. H. Casey and L. J. Crossey, Pittsburgh, 1996, pp. 113–120.
16 D. Burgard, R. Nass and H. Schmidt, *Werkstoffwoche, Symp. 6 Werkstoff und Verfahrenstechnik*, 1997, pp. 569–577.
17 D. Burgard, C. Kropf, R. Nass and H. Schmidt, *MRS 346: Better Ceramics through Chemistry IV*, ed. A. K. Cheetham, C. J. Briuker, M. L. Mecartney and C. Sanchez, Pittsburgh, 1994, pp. 101–107.
18 IUPAC, *Pure Appl. Chem.*, 1985, **57**, 603.
19 C. V. Santilli, S. H. Pulcinelli and D. F. Craievich, *Phys. Rev. B*, 1995, **51**, 8801.
20 J. Pütz, D. Ganz, G. Gasparro and M. A. Aegerter, *J. Sol–Gel Sci. Technol.*, in press.

Paper 8/05082A